The Hamilton-Jacobi partial differential equation and the three representations of traffic flow

Jorge A. Laval[a,*], Ludovic Leclercq[b]

[a] *School of Civil and Environmental Engineering, Georgia Institute of Technology*
[b] *Laboratoire Ingénierie Circulation Transport LICIT/ENTPE, Université de Lyon*

Abstract

This paper applies the theory of Hamilton-Jacobi partial differential equations to the case of first-order traffic flow models. The traffic flow surface is analyzed with respect to the three 2-dimensional coordinate systems arising in the space of vehicle number, time and distance. In each case, the solution to the initial and boundary value problems are presented. Explicit solution methods and examples are shown for the triangular flow-density diagram case. This unveils new models and shows how a number of existing models are cast as special cases.

Keywords: Hamilton-Jacobi partial differential equation, stochastic traffic flow, kinematic wave model

1. Introduction

The link between conservation laws and the Hamilton-Jacobi partial differential equation (HJ-PDE) has been known to mathematicians for decades (Lax, 1957; Olejnik, 1957; Hopf, 1970), but was brought up to the attention of the traffic flow theory community just recently by Daganzo (2005a,b, 2006a). This link implies that the kinematic wave model of Lighthill and Whitham (1955); Richards (1956) can be solved using its HJ-PDE formulation, which is much simpler to compute because the entropy solution is given automatically. In addition, when the fundamental diagram is bilinear

*Corresponding author. Tel. : +1 (404) 894-2360; Fax : +1 (404) 894-2278
Email address: jorge.laval@ce.gatech.edu (Jorge A. Laval)

numerical solutions become exact in the HJ framework, and this is not the case in the conservation law approach (LeVeque, 1993).

In this paper, the three-dimensional traffic flow surface that gives the vehicle number in time and space (Makigami et al., 1971) is analyzed with respect to the three possible 2-dimensional coordinate systems. This gives rise to three alternative solution methods to obtain the same surface, each one having advantages and disadvantages depending on the question being asked. Although special cases of these models have been published before (e.g., Newell, 2002, 1993; Mahut, 2000; Mahut et al., 2003; Daganzo, 2006b,a; Leclercq et al., 2007; Claudel and Bayen, 2010; Mazar et al., 2011; Leclercq and Becarie, 2012), this paper casts most of them in both general and specialized form under the Hamilton-Jacobi umbrella. In addition, the new discrete models do not require memory and are more flexible than existing ones, which allows for more efficient computer implementation.

This paper is organized as follows. Section 2 presents a brief background on the Hamilton-Jacobi PDE using the conventions in traffic flow theory. Section 3 applies this theory for the three coordinate systems considered here in the case of continuous fundamental diagrams. Piecewise-linear fundamental backgrounds are treated in section 4, while the special case of the triangular flow-density diagram is addressed in section 5. Finally, section 6 presents a brief discussion.

2. Preliminaries

The Hamilton-Jacoby partial differential equations expresses the evolution of a "quantity" $U(a, b)$ over dimensions a and b. The main requirement is that there exists a function $\mathcal{H}(\cdot)$–called the Hamiltonian or fundamental diagram in traffic flow–that gives one partial derivatives in terms of the other. If boundary data $G(\cdot)$ is given on a arbitrary curve $\mathcal{B}$ then the HJ-PDE reads:

$$\textbf{HJ} \begin{cases} U_a - \mathcal{H}(U_b, a, b) = 0, & \text{(1a)} \\ U(B) = G(B), \qquad B \in \mathcal{B} & \text{(1b)} \end{cases}$$

were subscript variables represent partial derivatives, B is a point with coordinates (a_B, b_B) in the boundary $\mathcal{B}$, and $G(B) \equiv G(a_B, b_B)$ is continuous. The solution of (1), known as the Hopf-Lax formula (Lax, 1957; Hopf, 1970),

involves the extrema of the function $\phi(\cdot)$:

$$\phi(B, \xi_{BP}; P) = G(B) + \int_{a_B}^{a} \mathcal{L}\left(\xi'_{BP}(y)\right) dy, \tag{2}$$

which is the sum of boundary data and the "cost" along path ξ_{BP} between point B and $P \equiv (a, b)$. The semicolon is used to emphasize that the generic point P is given and therefore not a variable. The quantity $\xi'_{BP}(a)$ is the slope of ξ_{BP} and the Lagrangian $\mathcal{L}(\cdot)$ is the Legendre transform of the Hamiltonian. Their definition depend on the curvature of $\mathcal{H}$, and on the numbering convention in traffic flow; see §3.1.

Hereafter we restrict our attention to homogeneous problems, i.e. $\mathcal{H} = \mathcal{H}(U_b)$, which implies that optimal paths are straight lines of slope $q_{BP} \equiv \xi'_{BP}(a)$. Therefore, (2) can be simplified to:

$$\phi(B; P) = G(B) + (a - a_B)\mathcal{L}\left(q_{BP}\right). \tag{3}$$

The particular solution formulae depends on the convexity of the Hamiltonian, as shown next.

2.1. Concave $\mathcal{H}$

If $\mathcal{H}(\cdot)$ is concave then

$$q_{BP} = (b - b_B)/(a - a_B) \tag{4}$$

is the slope of BP, and the solution of (1) is given by:

$$U(P) = \min_{B \in \mathcal{B}^P} \phi(B, P), \qquad \text{(solution for concave } \mathcal{H}\text{)} \tag{5a}$$

$$\mathcal{L}(q) = \max_{p} \{\mathcal{H}(p) - pq\}, \tag{5b}$$

where the auxiliary variable p refers to the argument of the Hamiltonian, i.e. $p \equiv |U_b|$, and $\mathcal{B}^P$ is the admissible region for B, defined momentarily.

For (5) to be the unique solution of (1) it is necessary that the extrema in (5b) be achieved at a single value of p, i.e. that the solution of

$$\mathcal{H}'(p) = q \tag{6}$$

be unique in p. This is guaranteed in the case of traffic flow because the Hamiltonian's curvature does not change sign within the range of admissible (i.e., physically meaningful) values for p. Thus, we can write

$$\mathcal{L}(q) = \mathcal{H}(p) - pq, \qquad p \Leftrightarrow \mathcal{H}'(p) = q \tag{7}$$

Since (6) is a one-to-one mapping between q and p, one can define the admissible range for $q, \mathcal{A}^q \equiv (\breve{q}, \hat{q})$, where $\breve{q} = \min_p\{\mathcal{H}'(p)\}$ and $\hat{q} = \max_p\{\mathcal{H}'(p)\}$. This defines the domain of dependence of point P, called $\mathcal{D}^P$, which gives all points to the left of P that can be connected to P by a straight line of slope $q \in \mathcal{A}^q$. Finally, $\mathcal{B}^P = \mathcal{B} \cap \mathcal{D}^P$ as shown in Fig. 4.

Another consequence of (6) is a duality relationship between $\mathcal{H}(\cdot)$ and $\mathcal{L}(\cdot)$, in the sense that one is the Legendre transform of the other, i.e. (5b) and

$$\mathcal{H}(p) = \min_q\{\mathcal{L}(q) + pq\}, \qquad \text{or:} \tag{8}$$

$$\mathcal{H}(p) = \mathcal{L}(q) + pq, \qquad q \Leftrightarrow \mathcal{L}'(q) = -p \tag{9}$$

2.2. Convex $\mathcal{H}$

If $\mathcal{H}(\cdot)$ is convex then

$$q_{BP} = -(b - b_B)/(a - a_B). \tag{10}$$

The appendix shows that the solution of (1) is given by:

$$U(P) = \max_{B \in \mathcal{B}^P} \phi(B, P), \qquad \text{(solution for convex } \mathcal{H}) \tag{11a}$$

$$\mathcal{H}(p) = \max_q\{\mathcal{L}(q) + pq\} \tag{11b}$$

$$\mathcal{L}(q) = \min_p\{\mathcal{H}(p) - pq\}. \tag{11c}$$

Note that (7) and (9) remain valid. For more details the reader is referred to (Evans, 1998, chapter 3), where the proofs for (5) for the initial value problem can be found.

3. The three representations of traffic flow

In traffic flow the quantity $U(a, b)$ may have three interpretations:

- $N(t, x)$: number of vehicles that have crossed location x by time t,
- $T(n, x)$: time vehicle n crosses x, and
- $X(t, n)$: position of vehicle n at time t.

$U(a,b)$	$N(t,x)$		$T(n,x)$		$X(t,n)$	
partials	N_t	$-N_x$	T_n	T_x	X_t	$-X_n$
symbol	$f(t,x)$	$k(t,x)$	$h(n,x)$	$r(n,x)$	$v(t,n)$	$s(t,n)$
name	flow	density	headway	pace	speed	spacing

Table 1: Coordinate systems and variables definition for the three representations

All these representations correspond to the same surface in the three-dimensional space of vehicle number, time and distance, but expressed with respect to the three coordinate systems: Eulerian coordinates (t, x), Lagrangian coordinates (n, x), and (t, n)[1]. Each coordinate system gives a different "model" to solve the same problem; these models are called the N-, T- or X-model hereafter. Our analysis is restricted to positive values for n, t, x.

3.1. Numbering convention and definitions

For the construction of these surfaces it is customary to impose that vehicle counts start with the same reference vehicle $n = 1$ at all locations. This convention implies that the density and spacing are the negative partial derivatives of their corresponding $U(a, b)$. This is shown in Table 1, which summarizes the meaning and symbols used here for partial derivatives in each coordinate system.

Table 2 summarizes the key definitions for each coordinate system in the context of HJ-PDE theory. For simplicity, we shall use the same symbol $\mathcal{H}, \mathcal{L}, \mathcal{B}, p, q, \ldots$ etc for all coordinate systems, but their specific meaning in each case are those in Table 2. The auxiliary variable p is forced to be positive to facilitate its interpretation.

[1]The other three possible coordinate systems can be omitted: it turns out that the fundamental diagram in (x, t) and (x, n) are not single-valued functions; (n, t) is equivalent to (t, n) since initial value problems in one correspond to boundary value problems in the other

	$N(t,x)$	$T(n,x)$	$X(t,n)$
HJ-PDE	$f = F(k)$	$h = H(r)$	$v = V(s)$
$\mathcal{H}(p)$	$F(k)$	$H(r)$	$V(s)$
$\mathcal{L}(q)$	$\max_k\{F(k) - k\tilde{v}\}$	$\min_r\{H(r) - r\tilde{s}\}$	$\max_s\{V(s) - s\tilde{f}\}$
$\mathcal{L}'(q)$	< 0	< 0	< 0
$\mathcal{L}''(q)$	≥ 0	≤ 0	≥ 0
$\mathcal{H}''(p)$	≤ 0	≥ 0	≤ 0
$p = \lvert U_b\rvert$	k	r	s
$q = \mathcal{H}'$	$\tilde{v}$, wave speed	$\tilde{s}$, wave spacing	$\tilde{f}$, wave flow
$\mathcal{B}^P_{\text{IVP}}$	$(x - \hat{q}t, x - \breve{q}t)^+$	$(x - \hat{q}n, x - \breve{q}n)^+$	$(n - \hat{q}t, n - \breve{q}t)^+$
$\mathcal{B}^P_{\text{BVP}}$	$(0, t - x/\breve{q})^+$	$(0, n - x/\breve{q})^+$	$(0, t - n/\breve{q})^+$

Table 2: Key elements of the Hamilton-Jacobi theory for the three coordinate systems. The superscript "+" is introduced to indicate that if a term is negative it should be replaced by 0.

With all, the solution for the three models can be expressed as:

$$N(t,x) = \min_{B\in\mathcal{B}^P}\left\{G(t_B,x_B) + (t-t_B)\mathcal{L}\left(\frac{x-x_B}{t-t_B}\right)\right\} \tag{12a}$$

$$T(n,x) = \max_{B\in\mathcal{B}^P}\left\{G(n_B,x_B) + (n-n_B)\mathcal{L}\left(-\frac{x-x_B}{n-n_B}\right)\right\} \tag{12b}$$

$$X(t,n) = \min_{B\in\mathcal{B}^P}\left\{G(t_B,n_B) + (t-t_B)\mathcal{L}\left(\frac{n-n_B}{t-t_B}\right)\right\} \tag{12c}$$

Finding the extrema in (12) amounts to a non-linear optimization problem in two variables; e.g. for (12a), minimizing $\phi(B,P) = G(t_B,x_B)+(t-t_B)\mathcal{L}((x-x_B)/(t-t_B))$ with respect to t_B and x_B. Depending on the shape of $G(\cdot)$ and of the boundary $\mathcal{B}$, this problem may or may not have local extrema.

3.2. Boundary conditions

Hereafter we focus on the initial and boundary value problem (IBVP), which is the combination of the initial value problem and boundary value problem. For the initial value problem (IVP) the boundary $\mathcal{B}$ is the line $a_B = 0$, and for the boundary value problem (BVP) $\mathcal{B}$ is the line $b_B = 0$; their interpretation in each case is given in table 3. Notice from the table that the IBVP for the T- and X-model assume that there is no passing of the lead vehicle, e.g. on a single-lane facility. Passing on multi-lane facilities will be dealt with in section 5.1.

	IVP(initial value problem)	BVP(boundary value problem)
$N(t,x)$	$N(0,x)$: cumulative vehicle profile at $t=0$	$N(t,0)$: cumulative count curve at $x=0$
$T(n,x)$	$T(0,x)$: trajectory of the lead vehicle	$T(n,0)$: time every vehicle enters the freeway
$X(t,n)$	$X(0,n)$: position of all vehicles at $t=0$	$X(t,0)$: trajectory of the lead vehicle

Table 3: Interpretation of the data $G(\cdot)$ in IVPs and BVPs per model.

We call the function $\phi(B,P)$ to be maximized in each case ϕ_{IVP} and ϕ_{BVP} respectively, and their P-dependency will be omitted for simplicity. The admissible region for IVPs and BVPs, $\mathcal{B}^P_{\text{IVP}}$ and $\mathcal{B}^P_{\text{BVP}}$, is shown in Figs. 1a, 2a and 3a and given in Table 2.

In the case of the T-model, the function $\phi(B,P)$ for IVPs and BVPs read:

$$\phi_{\text{IVP}}(x_B) = G(x_B) + n\mathcal{L}\left(-\frac{x-x_B}{n_B}\right), B \in \mathcal{B}^P_{\text{IVP}} \tag{13a}$$

$$\phi_{\text{BVP}}(n_B) = G(n_B) + (n-n_B)\mathcal{L}\left(-\frac{x}{n-n_B}\right), B \in \mathcal{B}^P_{\text{BVP}} \tag{13b}$$

In both cases, the solution will be given by the first- and second-order conditions for an extrema: $\phi'_- = 0$ and $\phi''_- < 0$ for the T-model (the underscore is a placeholder for IVP or BVP). The reader can verify that the first-order conditions in each case ensure that (9) is satisfied at all candidates B; i.e., for IVPs this condition implies $L'(q) = -p$ and for BVPs, $\mathcal{H}(p) = \mathcal{L}(q) + pq$.

4. Piecewise-linear fundamental diagrams

In the generic (a,b)-space, a piecewise-linear fundamental diagram with $m-1$ pieces and vertices at $(\mathcal{H}_i, p_i), i = 1 \dots m$, and its related Lagrangian with vertices at $(\mathcal{L}_i, q_i), i = 1 \dots m-1$, can be expressed as:

$$\mathcal{H}(p) = \mathcal{L}_i + pq_i, \qquad p \in (p_i, p_{i+1}), \tag{14a}$$

$$\mathcal{L}(q) = \mathcal{H}_i - qp_i, \qquad q \in (q_i, q_{i-1}) \tag{14b}$$

whith $0 \le p_1 < p_2 < \ldots < p_m$; $q_1 > q_2 > \ldots > q_{m-1}$ for concave $\mathcal{H}(\cdot)$, and $q_1 < q_2 < \ldots < q_{m-1}$ for convex $\mathcal{H}(\cdot)$. See Fig. 5 for the N-model. Notice

from the figure's geometry that:

$$\mathcal{L}_i = \mathcal{H}_i - p_i q_i, \qquad i = 1 \dots m, \tag{15a}$$

$$\mathcal{L}_i = \mathcal{H}_{i+1} - p_{i+1} q_i, \qquad i = 1 \dots m-1. \tag{15b}$$

One can show that if $\mathcal{H}(\cdot)$ in one coordinate system is piecewise linear, then it will be so in all coordinate systems considered here. In all cases, the function to be extremized is analogous to (1); i.e.:

$$\phi(B;P) = G(B) + (a - a_B)\mathcal{L}_i \qquad B \in \mathcal{B}^P, q_{BP} \in (q_i, q_{i+1}) \tag{16}$$

It follows that finding the extrema in (16) reduces to a linear program if both the data $G(B)$ and boundary $\mathcal{B}^P$ are piecewise linear. This means that the number of candidate points that may be extrema is given by all points $B \in \mathcal{B}^P$ such that $q_{BP} = q_i, i = 1 \dots m-1$, in addition to the vertices in $G(B)$ and $\mathcal{B}^P$. It is convenient to express (16) as a function of the segment index i by using the definition of waves q_i to eliminate B from (16); i.e.,

$$\phi^i_{\text{IVP}} = G(0, b \pm a q_i) + a\mathcal{L}_i, \tag{17a}$$

$$\phi^i_{\text{BVP}} = G(a \pm b/q_i, 0) \pm (b/q_i)\mathcal{L}_i \tag{17b}$$

where $\pm$ is "+" for the T-model (where $q_i = -(b - b_B)/(a - a_B)$), and "$-$" for the N- and X-models. For the T-model, for instance, characteristic slopes q_i are the wave spacings $\tilde{s}_i$ (see Table 2). In particular, we have $\tilde{s}_i = -(x - x_B)/n$ for the IVP and $\tilde{s}_i = -x/(n - n_B)$ for the BVP. This gives:

$$\phi^i_{\text{IVP}} = G(0, x + n\tilde{s}_i) + n\mathcal{L}_i, \tag{18a}$$

$$\phi^i_{\text{BVP}} = G(n + x/\tilde{s}_i, 0) + (x/\tilde{s}_i)\mathcal{L}_i, \tag{18b}$$

Finally, we conclude that the IBVP solution for the T-model and linear data can be expressed as:

$$T(n,x) = \max\left\{\{\phi^i_{\text{BVP}}\}_{i=1}^{m-1}, \{\phi^i_{\text{IVP}}\}_{i=1}^{m-1}\right\} \tag{19}$$

where $\{\phi^i_-\}_{i=1}^{m-1}$ gives the list $\{\phi^1_-, \phi^2_-, \dots, \phi^{m-1}_-\}$. Recall that if the data and/or boundary in $\mathcal{B}^P$ are piecewise-linear one should incorporate the corresponding vertices to the list in (19).

The important case of a triangular flow-density diagram is examined next.

	$N(t,x)$			$T(n,x)$			$X(t,n)$		
i	1	2	3	1	2	3	1	2	3
p_i	0	k^*	κ	0	u^{-1}	∞	δ	s^*	∞
q_i	u	$-w$	$-$	$-\infty$	δ	$-$	$w\kappa$	0	$-$
$\mathcal{H}_i$	0	Q	0	∞	Q^{-1}	∞	0	u	u
$\mathcal{L}_i$	0	$w\kappa$	$-$	∞	τ	$-$	$-w$	u	$-$

Table 4: Parameter values when $m = 3$.

5. Triangular flow-density diagram

In this section we (i) specialize the results in the previous section to the case of triangular flow-density diagrams (m=3) for IBVPs, (ii) introduced bottlenecks, and (iii) derive exact screed models.

Fig. 1a shows a triangular flow-density fundamental diagram, which may be defined by its free-flow speed u, wave speed $-w$ and jam density κ. Other useful resulting parameters that will be used in the sequel are the capacity $Q = \kappa w u/(w + u)$, the critical density $k^* = Q/u$, the critical spacing $s^* = 1/k^*$, the jam spacing $\delta = 1/\kappa$ and the wave trip time between two consecutive vehicles $\tau = 1/(w\kappa)$. The corresponding fundamental diagrams for the T- and X-models are shown as solid bold lines in Figs. 2a and 3a, respectively. Table 4 summarizes the values of all parameters in the preciding section when $m = 3$.

5.1. General data

In this section the data $G(a, 0)$ and $G(0, b)$ for the IBVP are assumed to be general functions. Notice from table for that $q \in (q_1, q_2)$ and that Lagrangians $\mathcal{L}(q) = \mathcal{H}_2 - qp_2$ are linear in all cases; see Table 5. This reduces the number of optimal candidates very significantly. Most notably, the number of candidates for the BVPs is only one for all models; for the T-model IVP it is also one, while for the N- and X-models, it depends upon the shape of the initial data.

To see this, we examine the first derivative of the ϕ-function to be extremizad in each case, $\phi'_{\rm IVP}(y)$ and $\phi'_{\rm BVP}(z)$ for all models; see the last 2 rows in Table 5. Notice that for the T-model $\phi'_{\rm IVP}(y)$ is always non-negative, and that for all models $\phi'_{\rm BVP}(z)$ is either always non-positive or always non-negative. This implies that in these four cases the ϕ-function is either non-increasing or non-decreasing, and thus the optimum candidate is one of the limit values in $\mathcal{B}^P_{\rm IVP}$ or $\mathcal{B}^P_{\rm BVP}$. This is shown in part b of Fig. 1, 2 and 3.

	$N(t,x)$	$T(n,x)$	$X(t,n)$
$\mathcal{L}(q)$	$Q - k^*\tilde{v}$	$Q^{-1} - \tilde{s}/u$	$u - s^*\tilde{f}$
$\mathcal{A}^q$	$(-w, u)$	$(-\infty, \delta)$	$(0, \tau^{-1})$
$\mathcal{B}^P_{\text{IVP}}$	$(x - ut, x + wt)^+$	$(-\infty, x + n\delta)^+$	$(n - t/\tau, n)^+$
$\mathcal{B}^P_{\text{BVP}}$	$(0, t - x/u)^+$	$(0, n)$	$(0, t - n\tau)^+$
$\phi'_{\text{IVP}}(y)$	$k^* - k(0, y)$	$r(0, y) - u^{-1} \geq 0$	$s^* - s(0, y)$
$\phi'_{\text{BVP}}(z)$	$f(z, 0) - Q \leq 0$	$h(z, 0) - Q^{-1} \geq 0$	$v(z, 0) - u \leq 0$

Table 5: Key elements of the HJ theory in the case of a triangular flow-density diagrams.

Interestingly, it follows that, independently of the data $G(B)$, the IBVP solution of the T-model is given by (19), which has only two candidates in this case; see Fig. 2b:

$$T(n,x) = \max\left\{T(n,0) + x/u, T(0, x + n\delta) + n\tau\right\}. \tag{20}$$

The first term in brackets corresponds to (18b) with $i = 1$ and using the identity (15b) to find that $\mathcal{L}_1/q_1 = \mathcal{H}_2/q_1 - p_2 = p_2 = 1/u$; the second term is simply (18a) with $i = 2$. The graphical solution method associated with (20) in the time-space diagram is illustrated in Fig. 2c. The first term within the brackets of (20) is the dashed line of slope u in the figure, while the second term corresponds to the trajectory of the first vehicle shifted horizontally by $n\tau$ and vertically by $-n\delta$; note that $n\tau/n\delta = w$. Finally, vehicle n's trajectory is the lower envelope of these two curves.

The N- and X-model IBVP solutions with general data do not simplfy as much as in the T-model, because the sign of $\phi'_{\text{IVP}}(y)$ can change along the boundary; see Table 5. Therefore, there might be multiple candidates located anywhere in the IVP boundary; i.e.:

$$N(t,x) = \min\left\{\min_{y\in\mathcal{B}^P_{\text{IVP}}}\left\{N(0,y) + Qt - k^*(x-y)\right\}, N(t - x/u, 0)\right\} \tag{21}$$

$$X(t,n) = \min\left\{\min_{y\in\mathcal{B}^P_{\text{IVP}}}\left\{X(0,y) + ut - s^*(n-y)\right\}, X(t - n\tau, 0) - n\delta\right\} \tag{22}$$

after noting that $u\tau - s^* = -\delta$ in (22). The terms corresponding to the BVP (second terms in brackets) should be included only if the candidate is in $\mathcal{B}^P_{\text{BVP}}$; i.e., if $t - x/u \geq 0$ and $t - n\tau \geq 0$, respectively. Finally, when the initial data is linear the above recipes involve the minimum of two terms,

i.e.:

$$N(t,x) = \min\{N(0,x-ut), N(0,x+wt) + w\kappa t\} \tag{23a}$$

$$X(t,n) = \min\{X(0,n) + ut, X(0,n-t/\tau) - wt\} \tag{23b}$$

where we used $Qt - k^*(x-y) = w\kappa t$ when $y = x + wt$ in (23a)

5.2. Bottlenecks

Let $\xi_N(t)$ be the (moving) bottleneck trajectory in the time-space plane, $v_0(t) = \xi'_N(t)$ its speed, and f_D the flow downstream of the bottleneck when it is active (possibly a function of v_0). According to the theory of moving bottlenecks Newell (1993, 1998) the traffic states upstream, U, and downstream, D, of the bottleneck when it is active are connected by a straight line slope v_0 in the flow-density diagram; see Fig. 6a. The intercept of this line is the maximum bottleneck passing rate, $R(\cdot)$, defined as:

$$R(v_0, f_D) \equiv (1 - v_0/u) f_D. \tag{24}$$

Fig. 6b shows the moving bottlenecks theory in the fundamental diagram relevant to the X-model (pointed out in Leclercq et al. (2007)), where the bottleneck trajectory is the function $\xi_X(t)$ that gives the vehicle number that crosses the bottleneck at time t. Fig. 6c is for the T-model, where the trajectory $\xi_T(n)$ gives the location where vehicle n crosses the bottleneck. Using underscores "_" as placeholders for N, T and X, we notice that in all models: (i) the slope of the line connecting states D and U in the fundamental diagram is also ξ'_-, and (ii) the intercept of this line is the cost rate along ξ_-, and is denoted $\mathcal{L}_0(\xi'_-)$. Assuming that the bottleneck is active, one can show that the values for ξ'_- and $\mathcal{L}_0(\xi'_-)$ in each model are those summarized in table 6. Fig. 6d illustrates how the ξ_-'s are related under this assumption.

	$N(t,x)$	$T(n,x)$	$X(t,n)$
ξ'_-	v_0	$v_0/R(v_0,f_D)$	$R(v_0,f_D)$
$\mathcal{L}_0(\xi'_-)$	$R(v_0,f_D)$	$1/R(v_0,f_D)$	v_0

Table 6: Key elements of the moving bottlenecks theory for each model. The entries for the N- and X-model were pointed out in Daganzo (2005a); Leclercq et al. (2007).

As pointed out in Daganzo (2005a); Leclercq et al. (2007) in the context of the N- and X-model, bottlenecks (fixed and moving) can be added

as "shortcuts" to the solution network. In general, this corresponds to interpreting $\xi_-(\cdot)$ as an additional boundary whose data is not given but has to be calculated explicitly.

But this method fails when the bottleneck becomes inactive. Numerical solutions exist, however. In the N-model it suffices to impose that v_0 cannot be greater than downstream traffic speed (Laval and Daganzo, 2006; Leclercq et al., 2004). The T- and X-models have the added complication that $\xi'_T(n)$ depends on the state of the bottleneck: when the bottleneck is inactive the actual passing rate is no longer $R(v_0, f_D)$ but $R(v_0, f)$, where $f \leq f_D$ is the flow immediately upstream of the bottleneck. Leclercq et al. (2007) proposes a procedure to cope with this problem in the X-model; a similar method could be used in the T-model. It is a two-step method applied at each discrete point of the numerical method: First, assume the bottleneck is active and solve the model with the added shortcut. Second, identify which candidate produced the extremum: if it did not come from the bottleneck (i.e., it was inactive) identify f and update ξ_- accordingly.

Finally, we present the continuous T-model IBVP solution with an active bottleneck with constant v_0 and f_D. In this setting, $\xi'_T(n) = v_0/R(v_0, f_D)$ is also constant, and without loss of generality we take $\xi_T(0) = 0$. For points upstream of the bottleneck trajectory the solution is:

$$T(n,x) = \max\left\{T(n,0) + x/u, T_B + (n - n_B)\tau\right\} \tag{25}$$

where $B \equiv (n_B, x_B)$ is the candidate located at the bottleneck, $n_B = (x + n\delta)/(\delta + \xi'_T), x_B = n_B\xi'_T$ and $T_B = n_B/R(v_0, f_D)$. Similarly, the solution for points downstream of the bottleneck trajectory is:

$$T(n,x) = \max\left\{T_B + x/u, T(0, x + n\delta) + n\tau\right\} \tag{26}$$

where now $n_B = n, x_B = x + n\delta$.

5.3. Exact Discrete models

In this section the three continuous coordinate system in the previous sections are discretized in increments $\Delta n, \Delta t, \Delta x$. A "tilde" will denote a dimensionless quantity, e.g. $\widetilde{x} = x/\Delta x$ or $\widetilde{X}(\cdot) = X(\cdot)/\Delta x$. These dimensionless quantities are restricted to assume integer values only, and we will carefully choose the increments so that rounding operations are not needed. A necessary condition to accomplish this is:

$$\theta = \frac{u}{w} \quad \text{is an integer,} \tag{27}$$

which should be close to 6 or 7 for typical freeways (Ahn et al., 2003; Banks, 1989; Cassidy and Coifman, 1997).

Two types of discrete implementations are described here: (i) in a "lattice" implementation the coordinate system is discrete, e.g. $(\widetilde{t}, \widetilde{x})$, but the dependent variable is continuous, e.g. $X_{\widetilde{t},\widetilde{x}}$; (ii) in a cellular automata (CA) implementation everything is discrete, e.g. $\widetilde{X}_{\widetilde{t},\widetilde{x}}$. We use arguments in subscripts to emphasize that they are discrete variables.

The lattice implementation of the T-model can be obtained in two steps. First, we interpret the origin $(0, 0)$ in (20) and in Fig. 2b as $(n-\Delta n, x-\Delta x)$, which gives

$$T(n, x) = \max\{T(n, x - \Delta x) + \Delta x/u, T(n - \Delta n, x + \Delta n\delta) + \Delta n\tau\} \quad (28)$$

Second, we divide the arguments of $T(\cdot)$ by their respective increments. To ensure no numerical errors are introduced, the quantity $x + \Delta n\delta$ should be a lattice value, which can be achieved by choosing

$$\Delta x = \delta \Delta n \quad (29)$$

It follows that

$$T_{\widetilde{n},\widetilde{x}} = \max\{T_{\widetilde{n},\widetilde{x}-1} + \Delta x/u, T_{\widetilde{n}-1,\widetilde{x}+1} + \Delta x/w\} \quad (30)$$

is the lattice implementation of the T-model. Additionally, we can discretize time to obtain

$$\widetilde{T}_{\widetilde{n},\widetilde{x}} = \max\left\{\widetilde{T}_{\widetilde{n},\widetilde{x}-1} + \Delta x/(u\Delta t), \widetilde{T}_{\widetilde{n}-1,\widetilde{x}+1} + \Delta n\tau/\Delta t\right\} \quad (31)$$

This expression can be turned into a CA implementation by choosing:

$$\Delta t = \Delta x/u, \quad (32)$$

which gives the CA T-model:

$$\widetilde{T}_{\widetilde{n},\widetilde{x}} = \max\left\{\widetilde{T}_{\widetilde{n},\widetilde{x}-1} + 1, \widetilde{T}_{\widetilde{n}-1,\widetilde{x}+1} + \theta\right\} \quad (33)$$

This relationship is a well-defined CA because it is an operation that takes integer values and returns an integer. Notice that both the lattice and CA expressions (30) and (34) are independent of the discretization size Δn as

long as (29) and (32) are used. Also note that any sub-multiple of (29) such as $\Delta x = \delta \Delta n/c, c = 1, 2, \ldots$ also gives well-defined CA models:

$$\widetilde{T}_{\widetilde{n},\widetilde{x}} = \max\left\{\widetilde{T}_{\widetilde{n},\widetilde{x}-1} + 1, \widetilde{T}_{\widetilde{n}-1,\widetilde{x}+c} + c\theta\right\}, \tag{34}$$

which is convenient for its added flexibility. In particular, it allows us to use arbitrarily large Δn while keeping Δx reasonably small.

For the N- and X-models we can proceeding analogously to the T-model. Since in both cases time is a dimension, it is convenient to step in time by solving sequential IVPs with small enough mesh size so that the initial data can be assumed linear between lattice points. The reader can verify that the lattice N-model is:

$$N_{\widetilde{t},\widetilde{x}} = \min_{i=-1,0,\ldots\theta}\left\{N_{\widetilde{t}-1,\widetilde{x}-i} + \Delta n\frac{\theta - i}{\theta + 1}\right\} \tag{35}$$

with the following discretization: $\Delta x = \delta \Delta n, \Delta t = \tau \Delta n$ and arbitrary Δn. Note that since N is dimensionless, (35) can be interpreted also as a CA model with real-valued states; no CA with integer states can be formulated: the only possibility would be $\Delta n = (\theta + 1)$ but this implies that density is measured in units of jam density, which is unpractical. Notice that model (35) does not require memory.

For the X-model:

$$X_{\widetilde{t},\widetilde{n}} = \min\left\{X_{\widetilde{t}-1,\widetilde{n}} + \theta\Delta x, X_{\widetilde{t}-1,\widetilde{n}-1} - \Delta x\right\} \tag{36a}$$

$$\widetilde{X}_{\widetilde{t},\widetilde{n}} = \min\left\{\widetilde{X}_{\widetilde{t}-1,\widetilde{n}} + \theta, \widetilde{X}_{\widetilde{t}-1,\widetilde{n}-1} - 1\right\} \tag{36b}$$

with $\Delta n = \kappa \Delta x, \Delta t = \Delta x/w$ and arbitrary Δx. The free parameters in these models–i.e., Δn in (35) and Δx in (36)–allow more flexibility than customary in the literature, as shown in the next section.

5.4. Existing models

Existing models in the traffic flow literature can be cast as special cases of the models presented here.

To the authors' knowledge Mahut (2000); Mahut et al. (2003) was the first to propose a version of the T-model, which was derived from Newell's car-following model (Newell, 2002). It corresponds to the lattice T-model (30) using Δx equal to the link length. In this way, the model is only evaluated at link entry and exit points, which is convenient for dynamic traffic

assignment applications. The model in Leclercq and Becarie (2012) is similar to Mahut's, but it made the connection with variational theory and added moving bottlenecks and heterogeneous vehicle types.

Newell's three-detector method (Newell, 1993) is the N-model (21) with boundary values given at two locations, x_U and x_D, $x_U < x_D$. It was shown in the previous section that regardless of the model, there is only one candidate for the boundary value problem. Thus:

$$N(t,x) = \min\left\{N(t-(x-x_U)/u, x_U), N(t-(x-x_D)/w, x_D) + (x_D - x)\kappa\right\} \tag{37}$$

after noticing that $(t-t_D)\mathcal{L}(-w) = ((x_D-x)/w)(Q+k^*w) = (x_D-x)\kappa$. Newell's car-following model (Newell, 2002) is (23b) with $\Delta n = 1, t = \tau$. Daganzo's CF(L) and CA(L) models (Daganzo, 2006b) are obtained by using $c = 1, \Delta x = \delta$ in (36a) and (36b), respectively. The model in eq. (22) in Daganzo (2006a) corresponds to the lattice implementation of (37) using $\Delta x = u\Delta t, x_U = x - \Delta x, x_D = x + \Delta x$:

$$N_{\widetilde{t},\widetilde{x}} = \min\left\{N_{\widetilde{t}-1,\widetilde{x}-1}, N_{\widetilde{t}-\theta,\widetilde{x}+1} + \kappa\Delta x\right\} \tag{38}$$

Notice that the term $\widetilde{t}-\theta$ is inconvenient for practical applications with large networks because it implies the need for storing the state of the network for θ time-steps.

6. Discussion

This paper uses the theory of Hamilton-Jacobi PDEs to express the traffic flow surface with respect to the three possible 2-dimensional coordinate systems. This produces three alternative solution methods to obtain this surface. In the case of the triangular flow-density fundamental diagram, these methods are expressed in continuous, lattice and cellular automata form. The new numerical methods are appealing because compared to existing methods they do not require memory, are exact and the mesh can be chosen with more flexibility. This should be particularly useful for network models, which typically require memory.

The T-model appears particularly promising to formulate stochastic kinematic wave model solutions because it always involves comparing only two terms, and these terms are not correlated. Existing stochastic extensions are

based on the N-model, which quickly become untractable due to multiple possible IVP candidates and possible correlation in the BVP data (Laval et al., 2012; Laval and Chilukuri, 2013; Hofleitner et al., 2012). Notice that one could also have a "two-term" solution in the X-model by considering the same boundary conditions as the T-model (see Fig. 3d): lead vehicle ($n = 0$) trajectory and passage time of each vehicle at $x = 0, t_n$, i.e.:

$$X(t, n) = \min\left\{(t - t_n)u, X(0, t - n\tau) - n\delta\right\}. \tag{39}$$

It is worth pointing out that the corresponding three conservation laws can be obtained by differentiating (1) with respect to b, which gives:

$$k_t + F(k)_x = 0 \tag{40a}$$

$$r_n - H(r)_x = 0 \tag{40b}$$

$$s_t + V(s)_n = 0 \tag{40c}$$

These are the conservation laws corresponding to the N-, T- and X-models, respectively. Of course, (40a) is the familiar kinematic wave LWR model, while (40c) has appeared a few times in the literature as the kinematic wave model in Lagrangian coordinates (Leclercq et al., 2007). It appears that (40b) is new.

In closing, we note that source terms of the form $W(a, b)$ in the HJ formulation have to be tackled with the general framework for non-homogeneous problems. In this case:

$$\begin{cases} U_a - \mathcal{H}(U_b) = W(a, b), & \text{(41a)} \\ \qquad U(B) = G(B), \qquad B \in \mathcal{B} & \text{(41b)} \end{cases}$$

and the function function $\phi(\cdot)$ becomes:

$$\phi(B, \xi_{BP}; P) = G(B) + (a - a_B)\mathcal{L}\left(q_{BP}\right) + \int_{a_B}^{a} W(y, \xi_{BP}(y))dy \tag{42}$$

where $\xi_{BP}(\cdot)$ is a path between B and P, and $\xi'_{BP}(\cdot) \in \mathcal{A}^q$. Special cases for this problem are being currently investigated by the authors.

Acknowledgements

This research was supported by the GDOT research project 2006S18 and NSF Grant # 1055694. The authors acknowledge Bhargava Chilukuri, Danjue Chen and Jincheng Zhu for their valuable comments and help with the artwork.

References

Ahn, S., Cassidy, M., Laval, J. A., 2003. Verification of a simplified car-following theory. Transportation Research Part B 38 (5), 431–440.

Banks, J. H., 1989. Freeway speed-flow-concentration relationships: More evidence and interpretations. Transportation Research Record 1225, 53–60.

Cassidy, M., Coifman, B., 1997. The relation between average speed, flow and occupancy and the analogous relation between density and occupancy. Transportation Research Record (1591), 1–6.

Claudel, C., Bayen, A., may 2010. Lax-hopf based incorporation of internal boundary conditions into hamilton-jacobi equation. part ii: Computational methods. Automatic Control, IEEE Transactions on 55 (5), 1158 –1174.

Daganzo, C., December 2006a. On the variational theory of traffic flow: well-posedness, duality and applications. Networks and Heterogeneous Media 1 (4), 601–619.

Daganzo, C. F., 2005a. A variational formulation of kinematic wave theory: basic theory and complex boundary conditions. Transportation Research Part B 39 (2), 187–196.

Daganzo, C. F., 2005b. A variational formulation of kinematic waves: Solution methods. Transportation Research Part B: Methodological 39 (10), 934 – 950.

Daganzo, C. F., 2006b. In traffic flow, cellular automata = kinematic waves. Transportation Research Part B 40 (5), 396–403.

Evans, L. C., Jun. 1998. Partial Differential Equations (Graduate Studies in Mathematics, V. 19) GSM/19. American Mathematical Society.

Hofleitner, A., Claudel, C., Bayen, A., 2012. Probabilistic formulation of estimation problems for a class of hamilton-jacobi equations. In: 51st IEEE Conference on Decision and Control.

Hopf, E., 1970. On the right weak solution of the cauchy problem for a quasilinear equation of first order. Indiana Univ. Math. J. 19, 483–487.

Laval, J., He, J., Castrillon, F., 2012. Stochastic extension of newell's "three-detector method. Transportation Research Record: Journal of the Transportation Research Board 2315, 73–80.

Laval, J. A., Chilukuri, B. R., 2013. The distribution of congestion on a class of stochastic kinematic wave model. Transportation Science (Forthcoming).

Laval, J. A., Daganzo, C. F., 2006. Lane-changing in traffic streams. Transportation Research Part B 40 (3), 251–264.

Lax, P. D., 1957. Hyperbolic systems of conservation laws ii. In: Sarnak, P., Majda, A. (Eds.), Communications on Pure and Applied Mathematics. Wiley Periodicals, p. 537566.

Leclercq, L., Becarie, C., 2012. A meso lighthill-whitham and richards model designed for network applications. In: Proceedings of the 91st Transportation Research Board Annual Meeting (TRB), 21-26 January, Washington, (USA) [CDROM]. Washington: Transportation Research Board, 2012, 10p.

Leclercq, L., Chanut, S., Lesort, J., 2004. Moving bottlenecks in the LWR model : a unified theory. Transportation Research Record 1883, 3–13.

Leclercq, L., Laval, J., Chevallier, E., 2007. The Lagrangian coordinate system and what it means for first order traffic flow models. In: Heydecker, B., Bell, M., Allsop, R. (Eds.), 17th International Symposium on Transportation and Traffic Theory. Elsevier, New York.

LeVeque, R. L., 1993. Numerical methods for conservation laws. Birkhauser Verlag.

Lighthill, M. J., Whitham, G., 1955. On kinematic waves. I Flow movement in long rivers. II A theory of traffic flow on long crowded roads. Proceedings of the Royal Society of London 229 (A), 281–345.

Mahut, M., 2000. Discrete flow model for dynamic network loading. Ph.D. thesis, Dpartement dinformatique et de recherhe oprationelle, Universit de Montral, (Also published as Report CRT-2001-04, Center for Research on Transportation, University of Montreal.).

Mahut, M., Florian, M., Tremblay, N., 2003. Space-time queues and dynamic traffic assignment: A model, algorithm and applications. In: Proceedings of the Transportation Research Board 82nd Annual Meeting. Washington: TRB (DVD-Rom).

Makigami, Y., Newell, G., Rothery, R., 1971. Three-dimensional representation of traffic flow. Transportation Science 5, 302–313.

Mazar, P., Dehwah, A., Claudel, C., Bayen, A., 2011. Analytical and grid-free solutions to the lighthillwhithamrichards traffic flow model. Transportation Research Part B: Methodological 45, 1727–1748.

Newell, G. F., 1993. A simplified theory of kinematic waves in highway traffic, I general theory, II queuing at freeway bottlenecks, III multi-destination flows. Transportation Research Part B 27 (4), 281–313.

Newell, G. F., 1998. A moving bottleneck. Transportation Research Part B 32 (8), 531–537.

Newell, G. F., 2002. A simplified car-following theory : a lower order model. Transportation Research Part B 36 (3), 195–205.

Olejnik, O., 1957. Discontinuous solutions of non-linear differential equations. Translated by George Biriuk. Am. Math. Soc., Transl., II. Ser. 26, 95–172.

Richards, P. I., 1956. Shockwaves on the highway. Operations Research (4), 42–51.

Appendix A.

This appendix shows that if $\mathcal{H}(p)$ is convex then (11) is the solution of (1); i.e:

$$U(t,x) = \max_{B \in \mathcal{B}} \left\{ G_B + (t - t_B)\mathcal{L}\left(-\frac{x - x_B}{t - t_B} \right) \right\}. \tag{A.1}$$

The following proof is an adaptation of Evan's in (Evans, 1998, p. 128) for concave Hamiltonian. It is done in two steps, showing that $U_t - \mathcal{H}(U_x) \geq 0$ and $U_t - \mathcal{H}(U_x) \leq 0$.

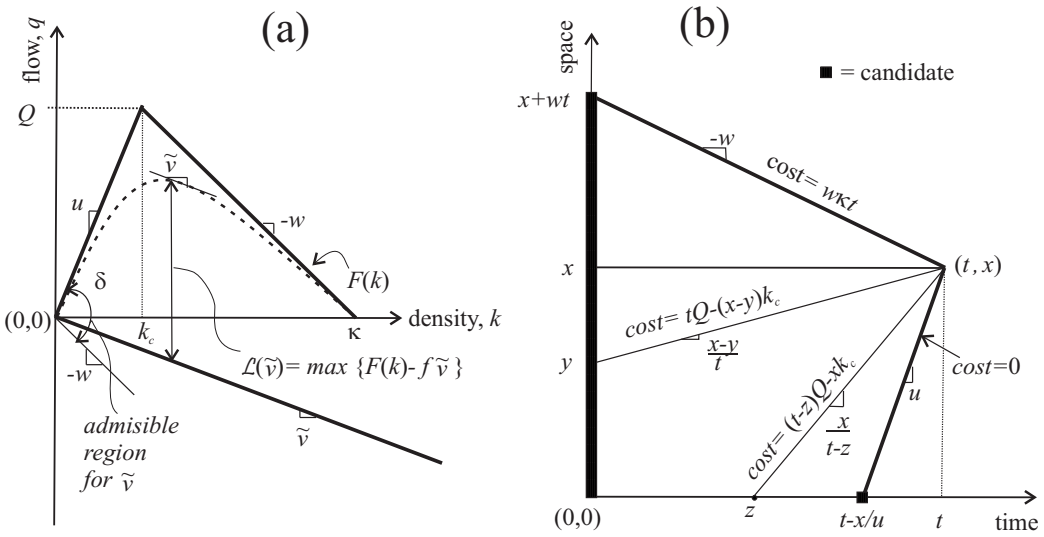

Figure 1: Illustrations for the N-model: (a) the triangular fundamental diagram (bold line), general concave fundamental diagram (dashed curve); (b) candidates and link costs for the IBVP with arbitrary data.

1) The solution at point $(t+h, x+hs), h, s > 0$, can be expressed as the solution of a HJ-IVP with data at time t:

$$U(t+h, x+hs) = \max_y \left\{ U(t,y) + h\mathcal{L}\left(-\frac{x+hs-y}{h} \right) \right\}.$$

Taking $y = x$ we have that $U(t+h, x+hs) \geq U(t,x) + h\mathcal{L}(-s)$. Hence,

$$\frac{U(t+h, x+hs) - U(t,x)}{h} \geq \mathcal{L}(-s).$$

We add and subtract $U(t+h, x)$ in the numerator to obtain

$$\frac{U(t+h, x+hs) - U(t+h,x) + U(t+h,x) - U(t,x)}{h} \geq \mathcal{L}(-s)$$

or equivalently,

$$s\frac{U(t+h, x+hs) - U(t+h,x)}{hs} + \frac{U(t+h,x) - U(t,x)}{h} \geq \mathcal{L}(-s). \quad \text{(A.2)}$$

Letting $h \to 0$ gives $sU_x(t,x) + U_t(t,x) \geq \mathcal{L}(-s)$, or

$$U_t - \mathcal{L}(-s) + sU_x \geq 0.$$

This expression is valid for all s, in particular for the value that satisfies (7), so that we can write $\mathcal{L}(-s) = \mathcal{H}(U_x) + sU_x$. This gives:

$$U_t - \mathcal{H}(U_x) \geq 0. \tag{A.3}$$

2) Now let $B^* \equiv (t^*, x^*)$ be the point in $\mathcal{B}$ that maximizes (A.1); i.e., $U(t,x) = G_{B^*} + (t - t^*)\mathcal{L}\left(-\frac{x-x^*}{t-t^*}\right)$. Fix $h > 0, d = t - h$ and let $z = x - hs^*$; i.e., the point (d, z) is on the line passing by (t^*, x^*) with slope $s^* = (x - x^*)/(t - t^*)$. Since s^* also equals $(z - x^*)/(d - t^*)$, and from (A.1) we have $U(d,z) \geq G_{B^*} + (d - t^*)\mathcal{L}(-s^*)$, then

$$U(t,x) - U(d,z) \leq G_{B^*} + (t - t^*)\mathcal{L}(-s^*) - (G_{B^*} + (d - t^*)\mathcal{L}(-s^*)) = h\mathcal{L}(-s^*)$$

It follows that

$$\frac{U(t,x) - U(t-h, x-hs^*)}{h} \leq \mathcal{L}(-s^*).$$

Similarly to how (A.2) was obtained, in this case we have

$$\frac{U(t,x) - U(t-h,x)}{h} + s^* \frac{U(t-h,x) - U(t-h, x-hs^*)}{hs^*} \leq \mathcal{L}(-s^*)$$

Letting $h \to 0$ gives $U_t(t,x) + s^* U_x(t,x) \leq \mathcal{L}(-s^*)$, or

$$U_t - (\mathcal{L}(-s^*) - s^* U_x) \leq 0. \tag{A.4}$$

But by (11b) it follows that $\mathcal{H}(U_x) \geq \mathcal{L}(-s^*) - s^* U_x$, and therefore (A.4) can be written as:

$$U_t - \mathcal{H}(U_x) \leq 0. \tag{A.5}$$

(A.3) and (A.5) complete the proof.

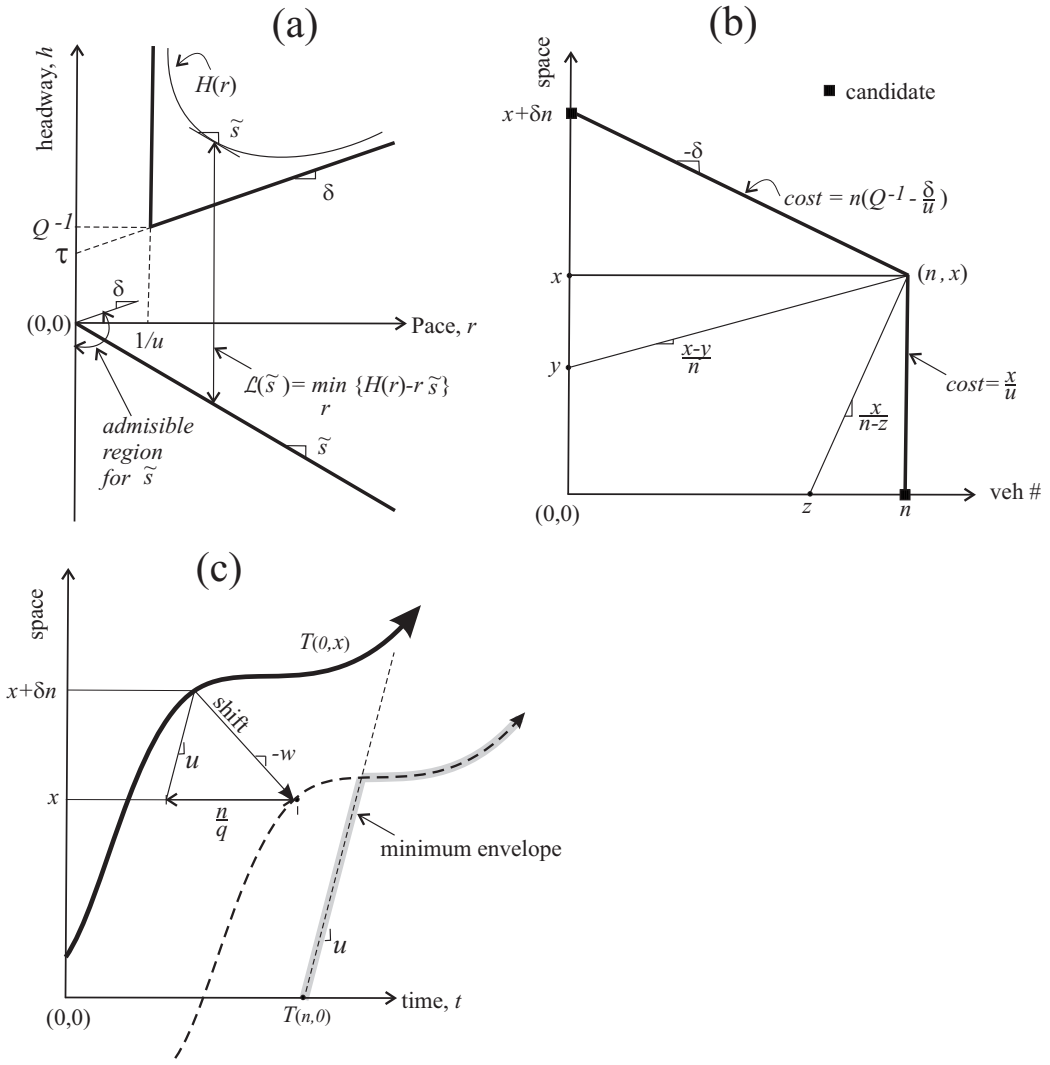

Figure 2: Illustrations for the T-model: (a) the Hamiltonian corresponding to the triangular flow-density fundamental diagram (bold line), general convex case (dashed curve); (b) candidates (only 2) and link costs for the IBVP with arbitrary data; (c) graphical solution method associated with (20) in the time-space diagram.

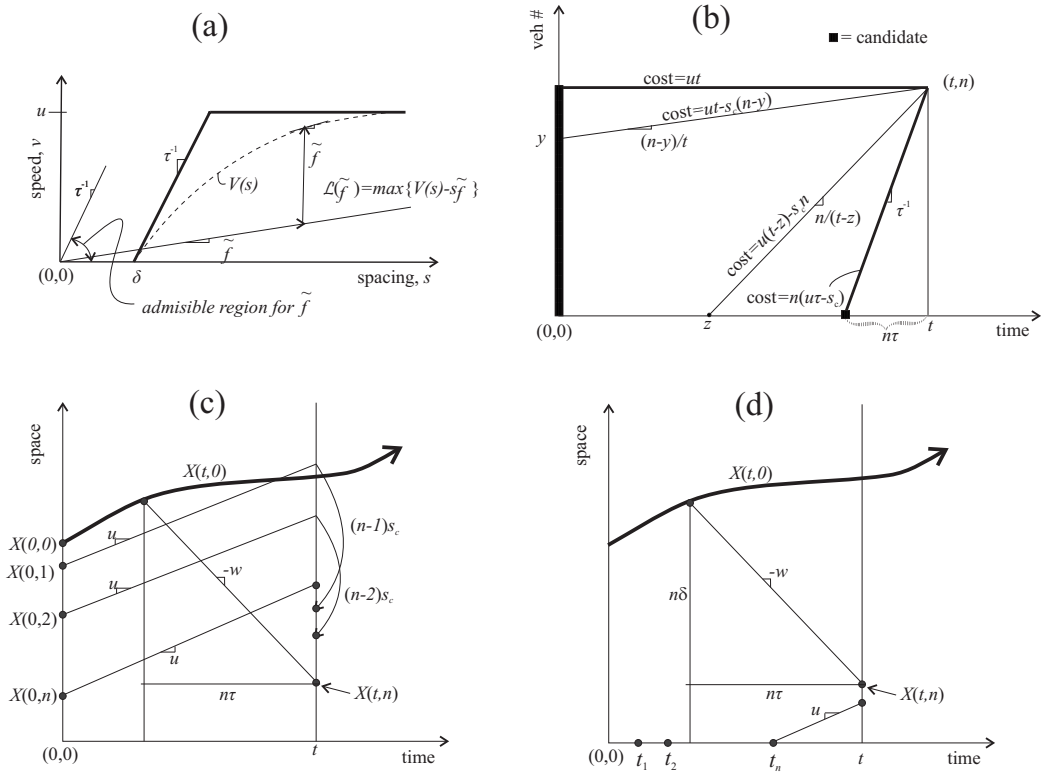

Figure 3: Illustrations for the X-model: (a) the Hamiltonian corresponding to the triangular flow-density fundamental diagram (bold line), general convex case (dashed curve); (b) candidates and link costs for the IBVP with arbitrary data; (c) graphical solution method associated with (22) in the time-space diagram; (d) X-model "two-term" solution with lead vehicle trajectory and passage time of each vehicle at $x = 0, t_n$, as boundary conditions.

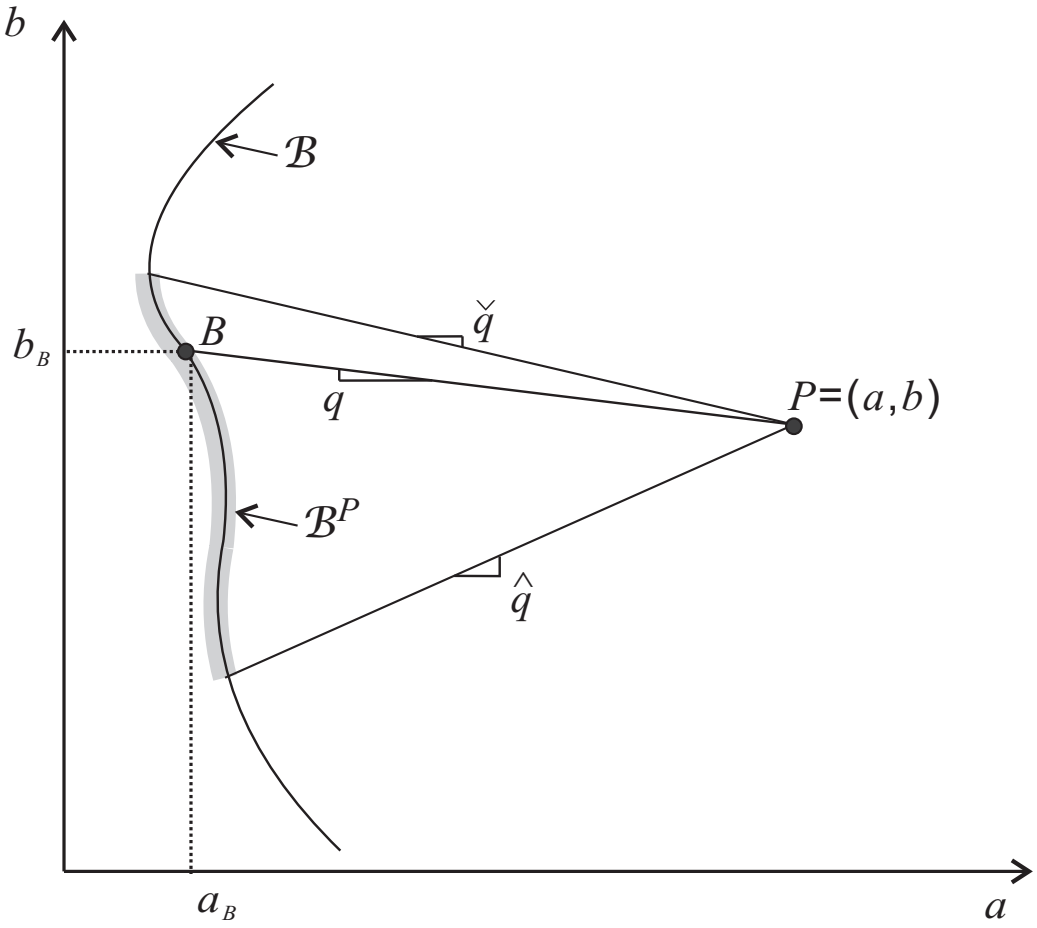

Figure 4: Some definitions in (a, b)-space when $\mathcal{H}$ is concave.

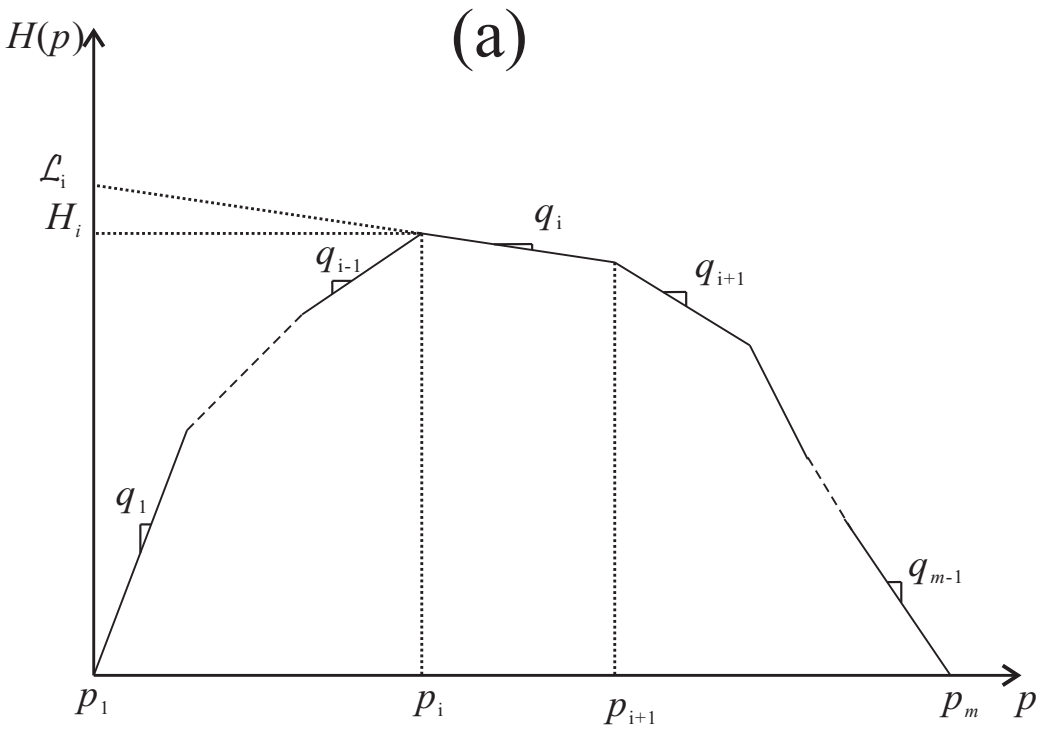

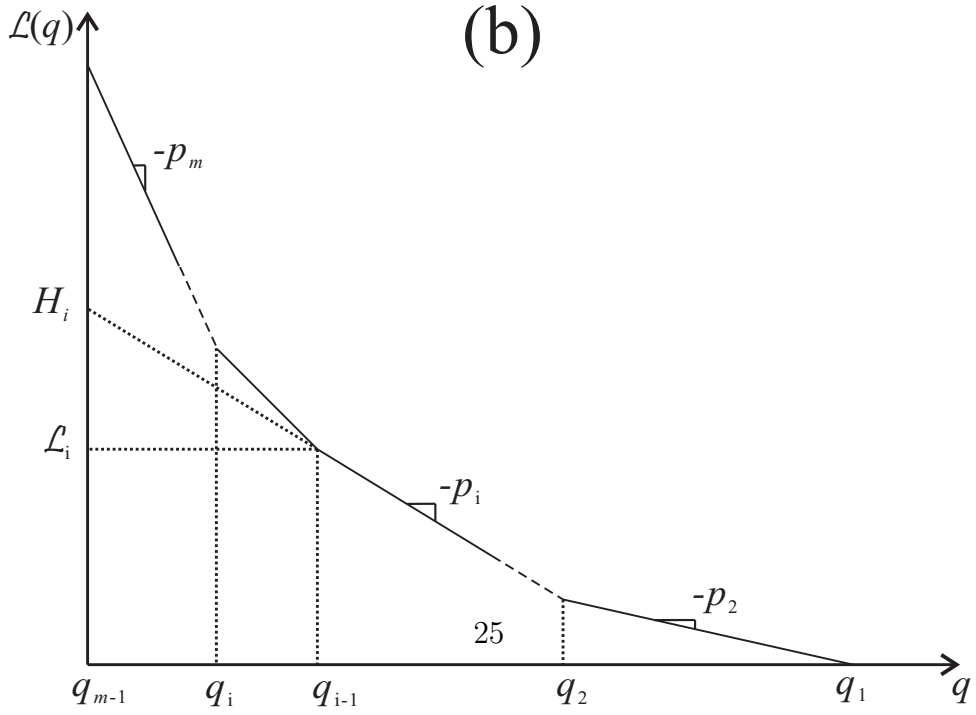

Figure 5: Piecewise-linear (a) fundamental diagram with m pieces and vertices at $(\mathcal{H}_i, p_i), i = 1 \ldots m+1$, (b) and its related Lagrangian with vertices at $(\mathcal{L}_i, q_i), i = 1 \ldots m$, in the case of the N-model.

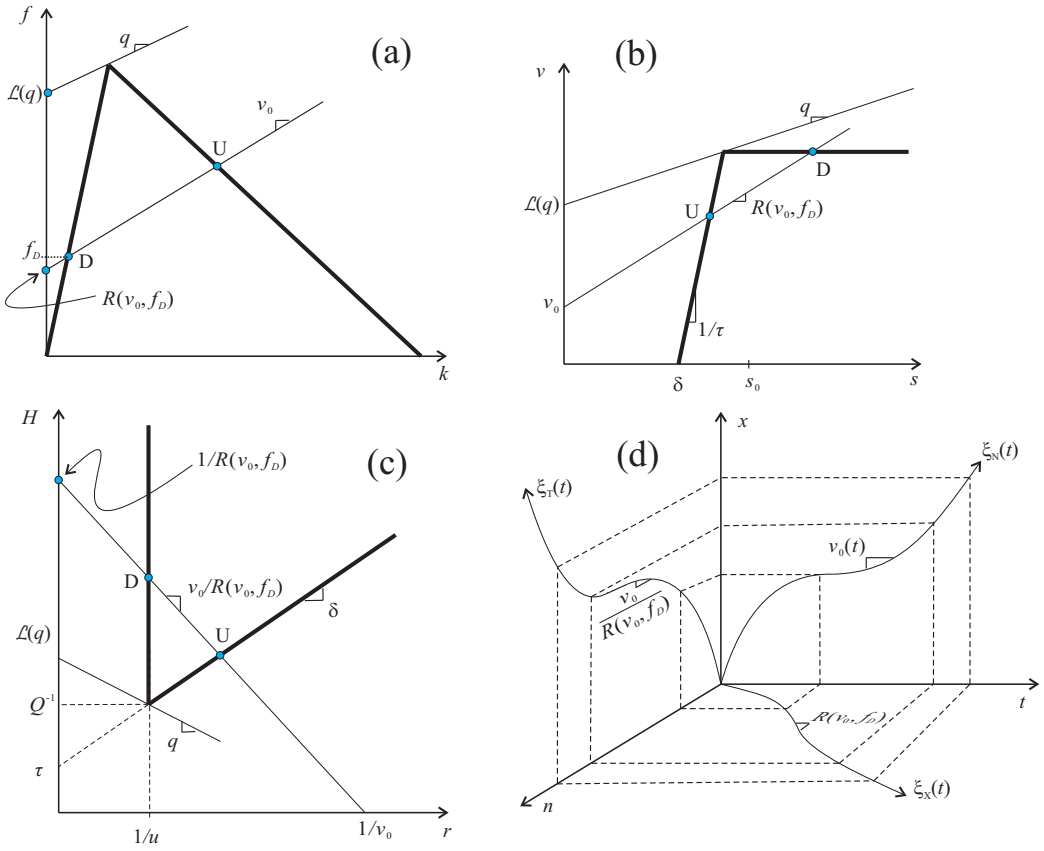

Figure 6: Moving bottlenecks theory in the fundamental diagram relevant to the (a) N-model, (b) X-model and (c) T-model; and (d) boundary conditions imposed by an active moving bottlenecks in each coordinate system.